Journal of Analytical and Applied Pyrolysis 125 (2017) 91–99

Contents lists available at ScienceDirect

Journal of Analytical and Applied Pyrolysis

journal homepage: www.elsevier.com/locate/jaap

High temperature SU-8 pyrolysis for fabrication of carbon electrodes

Y.M. Hassan[a,*], C. Caviglia[a], S. Hemanth[a], D.M.A. Mackenzie[a], T.S. Alstrøm[a,b], D.H. Petersen[a], S.S. Keller[a]

[a] Department of Micro- and Nanotechnology, Technical University of Denmark, 2800 Kongens Lyngby, Denmark
[b] Department of Applied Mathematics and Computer Science, Technical University of Denmark, 2800 Kongens Lyngby, Denmark

ARTICLE INFO

Keywords:
Pyrolytic carbon
Photoresist
Pyrolysis
Resistivity
Electrochemistry

ABSTRACT

In this work, we present the investigation of the pyrolysis parameters at high temperature (1100 °C) for the fabrication of two-dimensional pyrolytic carbon electrodes. The electrodes were fabricated by pyrolysis of lithographically patterned negative epoxy based photoresist SU-8. A central composite experimental design was used to identify the influence of dwell time at the highest pyrolysis temperature and heating rate on electrical, electrochemical and structural properties of the pyrolytic carbon: Van der Pauw sheet resistance measurements, cyclic voltammetry, electrochemical impedance spectroscopy and Raman spectroscopy were used to characterize the pyrolytic carbon.

The results show that the temperature increase from 900 °C to 1100 °C improves the electrical and electrochemical properties. At 1100 °C, longer dwell time leads to lower resistivity, while the variation of the pyrolysis parameters has small influence on electrochemical performance.

1. Introduction

Carbon electrodes have been widely studied due to their favorable properties including wide electrochemical potential window, chemical inertness, low fabrication costs and electrocatalytic activity for many redox reactions [1]. For this reason, various carbon allotropes such as highly oriented pyrolytic graphite, graphene, carbon nanotubes and carbon films have been investigated for numerous electrochemical applications including electroanalysis [2], electrocatalysis [3,4] or energy conversion and storage [5,6]. In particular, thin conductive carbon films with thickenss below hundreds of micron can be obtained using a pyrolysis process. Based on the precursor material used, different fabrication methods are available such as the pyrolysis of gases [7], graphite oxides [8] or electro-grafted layers derived from diazonium [9]. A promising approach to obtain thin carbon films with well-defined geometries is based on the pyrolysis of lithographically patterned photoresists [10–13]. The advantage of this process is that it is simple, highly reproducible and offers the possibility to customize the final electrode design. The resulting carbon is structurally and electrochemically similar to glassy carbon, with a microstructure composed of both graphitic (sp^2 hybridization of C bonds) and amorphous (sp^3 hybridization of C bonds) zones [10,11,14,15].

Pyrolytic carbon obtained from photoresists has been used for example for the fabrication of micro-batteries [16,17], and due to its biocompatibility [18] also for biosensors [19–21], cell culturing and differentiation [22] and bioparticle sorting and manipulation using dielectrophoresis [23].

Previous studies showed that depending on the pyrolysis conditions, the graphitic content is modified and that consequently the electrical and electrochemical properties of the carbon can be changed [14,24,25]. The parameters to be varied include maximum pyrolysis temperature, heating rate, number of temperature steps, dwell time at the maximum temperature and gas composition inside the furnace. In general, it has been shown that processes with higher temperatures lead to pyrolytic carbon with lower resistivity and better electrochemical performance [10,14,25].

The typical process used to pyrolyze photoresists consists of a treatment at 900 °C in nitrogen or forming gas, with a heating rate of 10 °C/min. It has been reported that under these conditions parameters such as dwell time or heating rate have an effect on the porosity of the pyrolytic carbon [25,26]. Only a few authors have shown experiments performed at 1100 °C, which represents the highest temperature achievable in quartz based furnaces [14,25]. The results indicate that higher temperatures are beneficial for electrode properties. However, to date no detailed experimental study of electrode fabrication with photoresists precursors pyrolyzed at elevated temperature has been reported. Here, we systematically investigate the influence of the pyrolysis conditions at 1100 °C. The aim of the study was to achieve

* Corresponding author.
E-mail address: yamoh@nanotech.dtu.dk (Y.M. Hassan).

http://dx.doi.org/10.1016/j.jaap.2017.04.015
Received 11 November 2016; Received in revised form 17 April 2017; Accepted 19 April 2017
Available online 23 April 2017

low resistivity and improved electrochemical performance of pyrolytic carbon electrodes.

The pyrolysis temperature (1100 °C), the gas environment (N_2) and number of temperature steps (one-step) were defined as fixed parameters in our study. The effects of different heating rates and dwell times at the maximum temperature were investigated. These two parameters were chosen to perform a central composite experimental design to investigate their influence on the electrical and electrochemical properties of the carbon electrodes.

Resistivity of the pyrolytic carbon was measured with a custom-made four terminal setup using the Van der Pauw (VdP) method [27,28]. The electrochemical behavior was evaluated with cyclic voltammetry (CV) and electrochemical impedance spectroscopy (EIS) using the redox couple ferri-ferrocyanide $[Fe(CN)_6]^{4-}/[Fe(CN)_6]^{3-}$, a commonly used probe to investigate the electrochemical properties of material surfaces.

2. Material and methods

2.1. Fabrication of pyrolytic carbon electrodes

Two different devices were designed and fabricated to characterize the pyrolytic carbon properties. 2D electrode chips were used to investigate the electrochemical properties. Custom-made square devices were used to perform Van der Pauw measurements and determine the electrical resistivity of the pyrolytic carbon films. The 2D electrode chips (10mm × 30 mm) consist of a three-electrode system where a circular carbon working electrode (WE) has an area of 12.5 mm^2 (Fig. 1A). The counter electrode has an area of 25.2 mm^2. The contact leads are made of a carbon layer (length 10 mm, width 700 µm) covered by Au with an adhesion layer of Ti or Cr (length 18 mm, width 1 mm) as shown in Fig. 1B. The Au pseudo-reference electrode (RE) has an area of 0.8 mm^2. Finally, the chip is covered by an insulating SU-8 passivation layer, except for the sensing area and the contact pads (Fig. 1C).The VdP devices have a 25 mm^2 area of pyrolytic carbon, surrounded by Au contacts as reported in Fig. 1D [28].

The fabrication process is illustrated in Fig. 2. 4-inch silicon wafers with 600 nm Si oxide grown by wet oxidation were used as substrates. First, the negative photoresist SU-8 2035 (Microresist GmbH) was dispensed manually and spin coated using a RCD8 spin coater (Süss MicroTec) (Fig. 2A and B). A two-step process was used to obtain a thickness of 17 µm: 1000 rpm for 10 s with an acceleration of 200 rpm/s followed by 5000 rpm for 120 s with an acceleration of 1000 rpm/s (Fig. 2B). Subsequently, the wafers were placed on a programmable hot plate (Harry Gerstigkeit GmbH) for soft bake (50 °C for 15 min) and then exposed using a chromium mask and a MA6/BA6 mask aligner with 365 nm wavelength (Süss MicroTec) in soft contact mode. The exposure dose used was 2 × 250 mJ/cm^2 with 30 s of waiting time between the two exposures (Fig. 2D). The development was performed in propylene glycol methyl ether acetate (PGMEA) using two subsequent immersions of 5 min each. The wafers were then rinsed with isopropanol and dried in air. An additional flood exposure step was performed to complete the crosslinking of the structures (2 × 250 mJ/cm^2 and 30 s of waiting time). Finally, the wafers were hard-baked for 15 h at 90 °C (Fig. 2E).

The pyrolysis of the SU-8 structures was performed in a PEO-604 furnace (ATV Technologie GmbH). Once the samples were pyrolyzed (Fig. 2F), 20 nm of titanium or chromium adhesion layer and 200 nm of gold were deposited by e-beam evaporation (Alcatel SCM 600) through a shadow mask to define the contact leads and pads (Fig. 2G).

Finally, to obtain 5 µm of passivation layer another lithography step was used. SU-2005 was spin coated at 2000 rpm for 30 s with an acceleration of 500 rpm/s. After solvent evaporation of 2 h at room temperature, the substrate was exposed using a chromium mask and a dose of 2 × 250 mJ/cm^2 with 30 s of waiting time. This was followed by a 1 h bake at 50 °C, rinse in PGMEA, flood exposure with the same parameters as the previous exposure and final hard bake of 15 h at 90 °C (Fig. 2H). The wafers were then cut using a dicing saw (Automatic Dicing Saw, DAD321, DISCO) to obtain single chips.

2.2. Design of experiment for investigation of pyrolysis conditions

The chosen parameters for the experimental design were the dwell time at the maximum temperature (t: 1 h, 3 h, and 5 h) and the heating rate (h: 10 °C/min, 30 °C/min, 50 °C/min). The experiment was carried out using a face centered central composite design [29] with full randomization and 2 center points resulting in 10 experimental runs in total. SAS JMP software package was used to analyze the results and identify the influence of the chosen parameters. The measured responses were resistivity, anodic peak current, peak potential separation ΔE_p and thickness after pyrolysis. Formally, the regression model used in the analysis was:

$$Y = \beta + a_1 t + a_2 h + a_3 th + a_4 t^2 + a_5 h^2 \quad (1)$$

where Y is either the resistivity, the anodic peak current, ΔE_p or thickness after pyrolysis, t is the dwell time and h is the heating rate. Hence four distinct models are fitted each with different intercept β and regression coefficients a_i. A factor is then defined significant if the corresponding regression coefficient is different from zero under the null hypothesis $H_0 : a_i = 0$ where the testing is carried out using the t-test.

The standard least squares approach was used to fit the data to the model. This method finds the response surface that minimizes the sum of the squares of the residuals of the points from the response surface.

For comparison with the state-of-the art process, the results of the characterization of electrodes fabricated at 900 °C (t: 2 h, h: 10 °C/min) have been included. As demonstrated in a previous optimization work at 900 °C, this process produced pyrolytic carbon with the best electrical and electrochemical properties at this temperature [30].

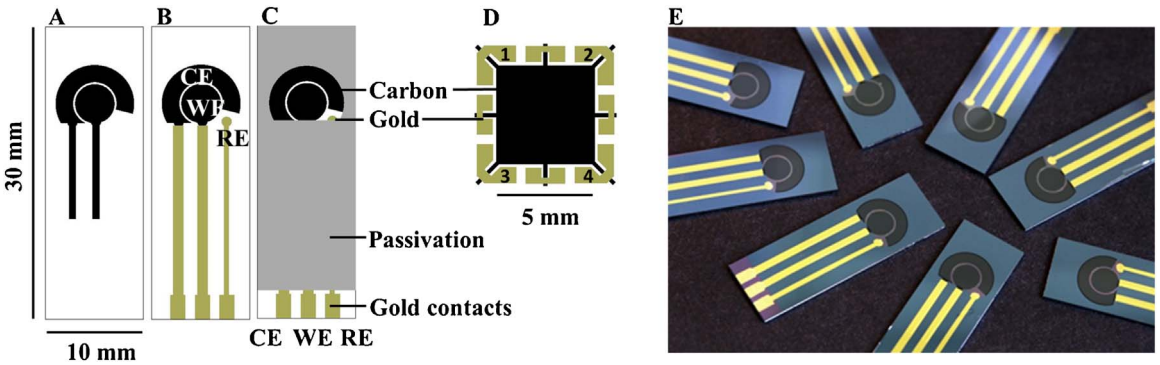

Fig. 1. Overview of 2D carbon electrodes: carbon layer (A), gold contact leads and pads (B), SU-8 passivation layer (C), Van der Pauw device for 4-point probe measurements (D), electrochemical electrodes (E).

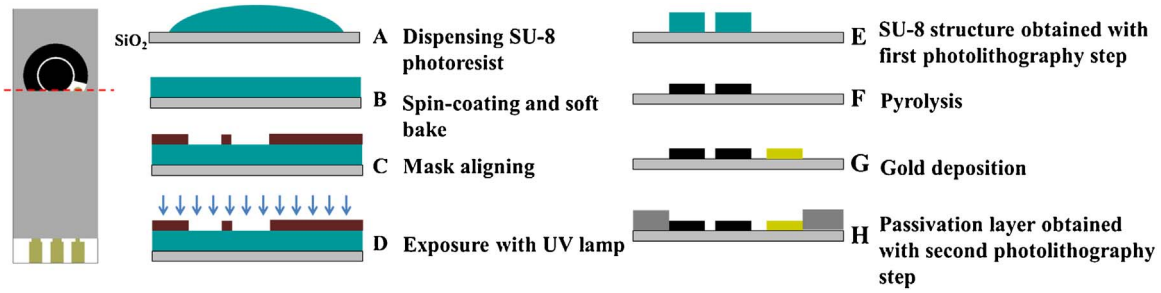

Fig. 2. Electrode fabrication process flow.

2.3. Structural characterization

The thickness of the carbon films was analyzed before and after pyrolysis using a stylus profiler (Dektak XTA, Bruker). Measurements were acquired in three different points on each sample and averaged. All the pyrolytic carbon films were characterized by Raman spectroscopy performed using a Raman microscope (DXR model, Thermo Fisher Scientific Inc.) with an excitation wavelength of 532 nm and 10 mW laser power. The obtained spectra were analyzed using the OMNIC software from Thermo Scientific and Matlab to perform a background correction. The roughness of carbon films was measured using Atomic force microscopy (AFM) using a DME dualscope DS 95 SPM (Danish Micro Engineering A/S, Denmark). The surface topography images of samples were acquired in tapping-mode with a silicon tip. Scan size was 5 µm × 5 µm.

2.4. Electrical characterization

The electrical characterization was performed with a custom-made four point resistance setup and the Van der Pauw method was used to measure the sheet resistance of the carbon films. The resistances R_A and R_C were measured in the electrode configuration defined in Fig. 1D as

$$R_A = \frac{V_{43}}{I_{12}}, R_C = \frac{V_{31}}{I_{24}} \quad (2)$$

To obtain a more precise measurement, the reciprocal values $R_A' = \frac{V_{21}}{I_{34}}$ and $R_C' = \frac{V_{42}}{I_{13}}$ were measured and $R_C$averaged with R_A and

The sheet resistance $R_S$was calculated using a Matlab algorithm in accordance to [27]

$$e^{\left(-\frac{\pi R_A}{R_S}\right)} + e^{\left(-\frac{\pi R_C}{R_S}\right)} = 1 \quad (3)$$

The resistivity was subsequently calculated multiplying the sheet resistance value by the carbon film thickness after pyrolysis.

2.5. Electrochemical characterization

The electrochemical characterization was performed on the 2D electrode chips using CV and EIS. The measurements were performed using a potentiostat (Autolab PGSTAT128N, Metronohm Autolab) and the software package NOVA was used to analyze the acquired data. The carbon electrode chips were subjected to an oxygen plasma treatment (0.5 bar) in an Atto Plasma System (Diener electronic) for 65 s with a power of 50 W to improve wettability [22]. The chips were subsequently placed in a PMMA-based self-aligning magnetic clamping system (Fig. 3) [31]. For every pyrolysis condition analyzed, three chips were used. CV and EIS measurements were acquired using 300 µl 10 mM ferri-ferrocyanide $[Fe(CN)_6]^{4-}/[Fe(CN)_6]^{3-}$ in phosphate buffered saline (PBS), both purchased from Sigma–Aldrich. Cyclic voltammograms were acquired using a three-electrode configuration and a scan rate of 100 mV in a potential range from −600 mV to 600 mV. EIS measurements were performed using a two-electrode configuration (WE and CE) acquiring data in the frequency range of 0.1–10^6 Hz, applying a sinusoidal potential of 10 mV and acquiring 10 points/decade.

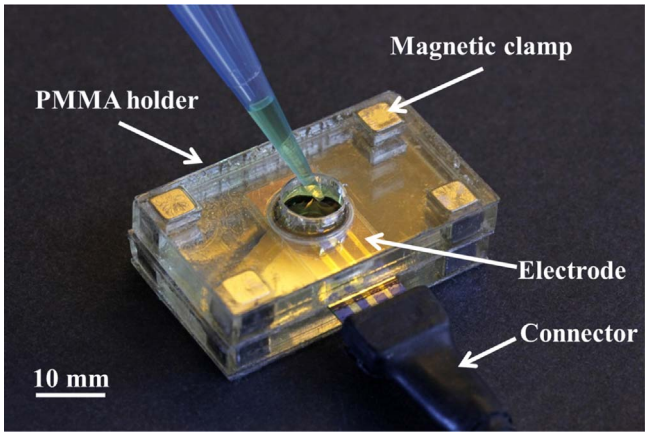

Fig. 3. Magnetic clamping system.

3. Results and discussion

The variables for the experimental design for the pyrolysis process were dwell time *t* and heating rate *h*. The four measured responses were resistivity, anodic peak current, peak potential separation ΔE_p and thickness after pyrolysis. For each factor, the terms that are statistically significant and thus have influence exhibit P-values lower than 0.05. To have an indication of the accuracy of the fitting, the coefficient of determination adjusted R^2 was calculated.

The P-values, adjusted R^2 values and parameter estimates for the regression coefficients a_i with 95% confidence interval are reported (see Supplementary Material, S1).

3.1. Thickness

Fig. 4 reports the thickness values after pyrolysis. The final thickness of the carbon electrodes for all the samples is below 2 µm, corresponding to a shrinkage above 80%. The results show that the heating rate was statistically significant with a P-value < 0.05 and an effect size of −4.83 ± 1.14 µm. Previous studies have shown that SU-8-derived carbon films obtained with different pyrolysis processes exhibit a decrease in height which is more prominent for an increase in the final pyrolysis temperature [12]. In our case, we show that also the heating rate can have a significant influence on the thickness after pyrolysis. For faster ramps there is less time for rearrangement of carbon bonds during the heating step. This might result in increased mass loss due to evaporation of organic compounds and consequently a more prominent decrease in final film thickness.

3.2. Raman spectroscopy

Raman spectroscopy was used to investigate the microstructure of

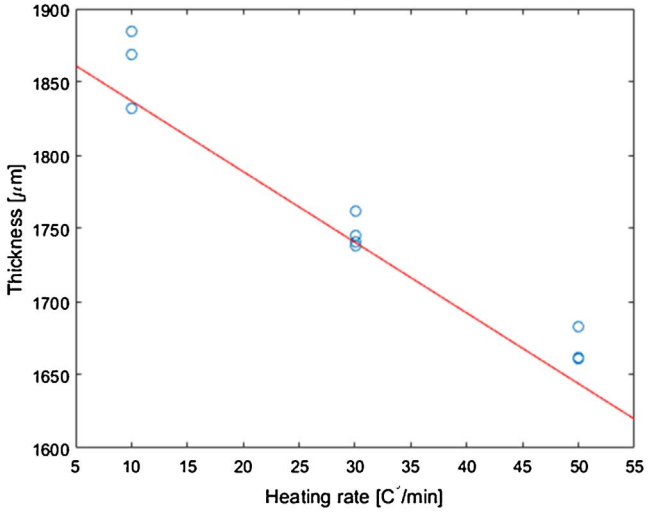

Fig. 4. Thickness measurements for pyrolytic carbon films obtained at 1100 °C using different dwell times in N_2 (1 h, 3 h, 5 h) and different heating rates (10 °C/min, 30 °C/min, 50 °C/min).

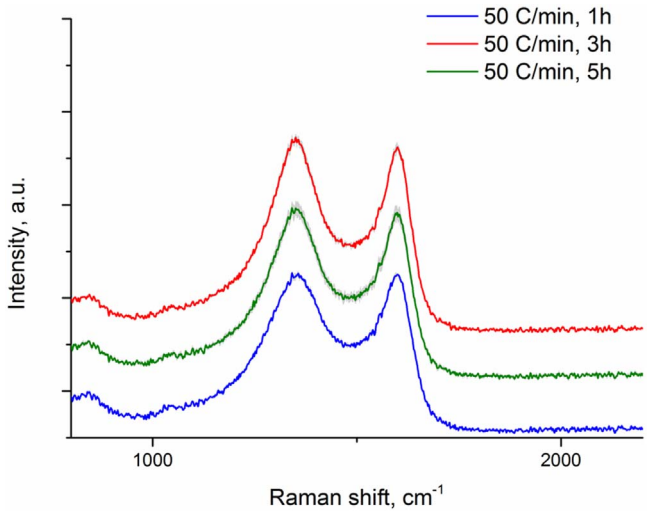

Fig. 5. Raman spectra of samples pyrolyzed at 1100 °C using different dwell times in N_2 (1 h, 3 h, 5 h) and heating rate of 50 °C/min. Data are presented as mean ± standard deviation (n = 3).

the pyrolytic carbon and identify variations in the graphitic content due to different pyrolysis processes. All the spectra acquired showed the typical graphitic band (G-band) and amorphous band (D-band), characteristic for carbon materials (Fig. 5) [32]. The G band at 1590 cm^{-1} is due to the E_{2g} vibration mode, related to the bond stretching of sp^2 hybridized C atoms present in the aromatic ring and olefinic chains [33]. The D band at 1330 cm^{-1} originates from the activation of the breathing mode of A_{1g} symmetry in sp^2C atoms and is related to defects and disorder in the graphite lattice[33]. It has been demonstrated that the ratio between the D peak and the G peak intensities is inversely proportional to the crystallite size L_a: $I_d/I_g \propto L_a$, where I_d and I_g are the intensities of the D and G peaks respectively [32]. The increasing value of this ratio, and thus a smaller L_a, is an indicator of an increasing disorder [33].

As shown in the representative Raman spectra reported in Fig. 5 and the values summarized in Table 1, the samples pyrolyzed at 1100 °C using different dwell times and heating rates in N_2 displayed similar I_d/I_g values. Different pyrolysis processes led to no measurable increase in the graphitic content, compared to the effects caused by a change of the final pyrolysis temperature [34].

Table 1
Values (average ± standard deviation, n = 3) of peak intensity ratio of the D and G peaks.

	Id/Ig
1 h,10 °C/min	1.10 ± 0.004
3 h,10 °C/min	1.02 ± 0.007
5 h,10 °C/min	1.03 ± 0.010
1 h,30 °C/min	0.99 ± 0.003
3 h,30 °C/min	1.00 ± 0.005
5 h,30 °C/min	1.01 ± 0.004
1 h,50 °C/min	0.99 ± 0.003
3 h,50 °C/min	1.05 ± 0.003
5 h,50 °C/min	1.02 ± 0.002

3.3. Resistivity measurements

Resistivity values are reported here in order to study the influence of the pyrolysis parameters on the electrical properties of pyrolytic carbon. Fig. 6A reports the resistivity values for pyrolytic carbon obtained at 1100 °C with different pyrolysis conditions compared with the resistivity value for pyrolytic carbon obtained at 900 °C. The temperature rise to 1100 °C leads to a significant decrease of resistivity from 9.3 ± 0.8 mΩcm for the 900 °C process to values lower than 4 mΩcm for all the investigated conditions at 1100 °C. These values are lower than other pyrolyzed photoresist films obtained with similar pyrolysis conditions: 6.8 mΩcm for SU-8 pyrolyzed at 1000 °C [25] and 5.1 mΩcm for AZ photoresist pyrolyzed at 1100 °C [11].

At 1100 °C the general trend is a decrease of the resistivity values when the dwell time is increased (Fig. 6B). This is confirmed by the data analysis of the design of experiments results (Supplementary Material S1), where it can be seen that the dwell time is the only statistically significant factor with a p-value of 0.04 and an effect size of −0.14 ± 0.13 mΩcm. In particular, the lowest resistivity values were obtained for t = 5 h processes with h = 10 °C/min and h = 50 °C/min: 3.18 ± 0.26 mΩcm and 3.24 ± 0.32 mΩcm respectively. Mardegan et al. showed a similar dwell time dependency at 900 °C, where electrodes pyrolyzed for the longest time of 4 h led to the lowest resistivity value measured [25]. Longer dwell times may provide longer time for the rearrangement of carbon atoms during the pyrolysis process and thus the formation of larger or differently oriented graphitic areas [25,35]. Alternatively, the lower resistivity for longer dwell times might be explained by partial annealing of the pyrolytic carbon film contributing to the formation of more graphitic carbon resulting in improved electrical properties. In related work, differences in the ratio between the graphitic (G) and amorphous (D) carbon peaks of Raman spectra have successfully been used to compare resistivity of samples pyrolyzed at different conditions [11]. However, as discussed above, the differences in Raman spectroscopy were insignificant in our studies. This indicates that the microstructural differences expected based on the electrical measurements are small and therefore could not be verified by Raman spectroscopy.

Focusing on the influence of the heating rate, the differences can be observed for the samples pyrolyzed with a heating rate of 10 °C/min and 50 °C/min, while there are no significant differences for the 30 °C/min ramp rate. However this parameter was not found statistically significant for the resistivity.

3.4. Cyclic voltammetry

The 2D chips described in Fig. 1C were used to characterize the electrochemical behavior of the pyrolytic carbon. The electrochemical characterization provides information about the electron transfer process and the interaction between electrode surface and electrolyte. CV with the redox couple ferri-ferrocyanide $[Fe(CN)_6]^{4-}/[Fe(CN)_6]^{3-}$ was used to evaluate and compare the performance of electrode chips

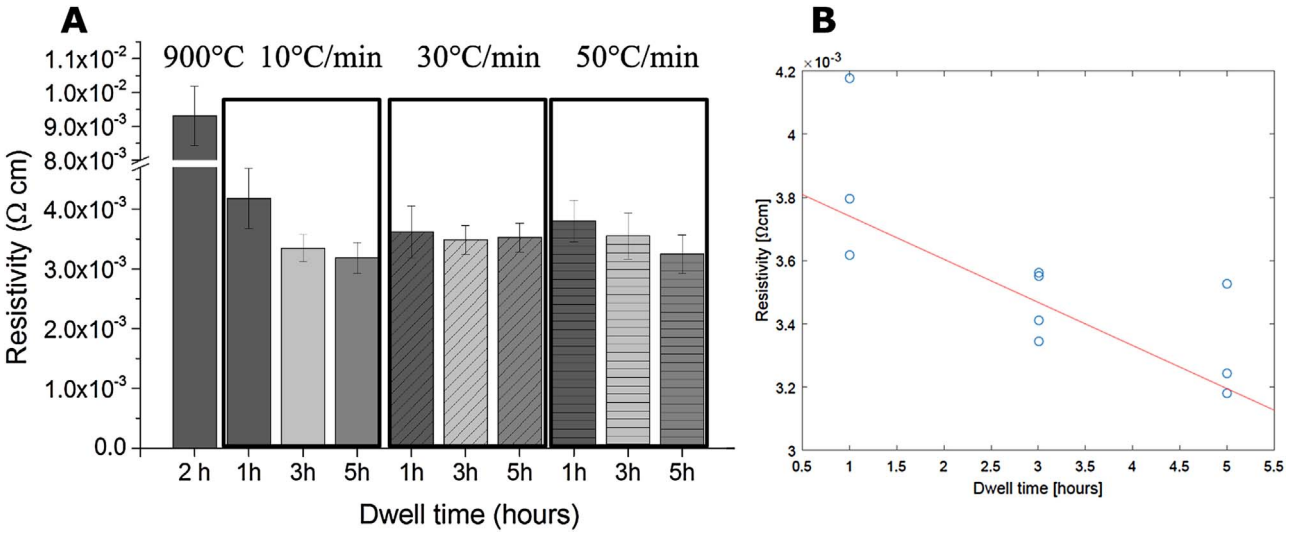

Fig. 6. Resistivity measurements for pyrolytic carbon films obtained at 1100 °C using different dwell times in N_2 (1 h, 3 h, 5 h) and different heating rates (10 °C/min, 30 °C/min, 50 °C/min). Comparison with pyrolytic carbon obtained at 900 °C (A) and influence of dwell time on resistivity values (B).

pyrolyzed under different conditions.

To identify the best electrochemical behavior, the first parameter taken into account was the peak current. According to the Randles-Sevcik equation, the anodic and cathodic peak current values in CVs vary if the electrode area, diffusion coefficient, redox species, concentration or voltage scan rate are varied [36]. Since in our case all the experimental parameters are constant, a higher peak current value indicates a lower electrode resistance. The second parameter taken into account was the ΔE_p, which for a reversible redox reaction is theoretically 59 mV. In principle, the optimal electrochemical behavior corresponds to large peak currents and low ΔE_p.

Fig. 7 reports representative voltammograms (h = 10 °C/min) comparing the electrochemical behavior for devices pyrolyzed at 900 °C and 1100 °C with the same heating rate but different dwell times. In Table 2 the values for the anodic peak current, cathodic peak current and ΔE_p for the different analyzed conditions are reported. As it can be seen, there is an increase in the peak currents and decrease of ΔE_p between electrodes obtained at 900 °C and 1100 °C. This is similar to what has been observed by others [10,11]. It can be explained by an improvement in the electron transfer due to a more conductive carbon fabricated at 1100 °C, as confirmed by the resistivity measurements.

At 1100 °C the voltammograms had a reproducible behavior, with small differences in peak current values and ΔE_p. The data analysis

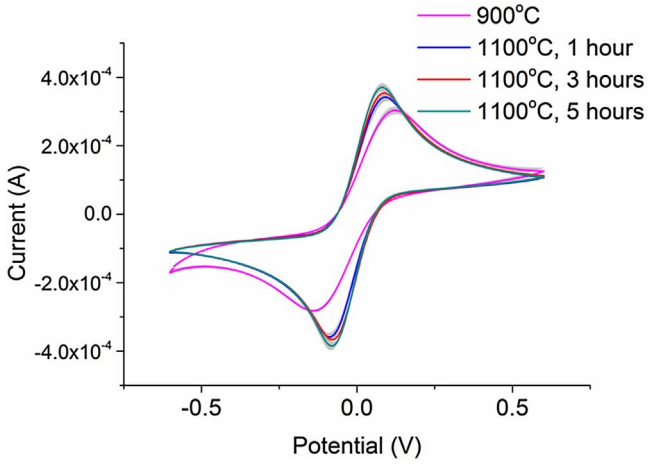

Fig. 7. Voltammogram of pyrolytic carbon electrodes obtained at 900 °C and 1100 °C with a heating rate of 10 °C/min acquired in 10 mM ferri-ferrocyanide with a scan rate 100 mV/s. Data are presented as mean ± standard deviation (n = 3).

Table 2
Values (average ± standard deviation, n = 3) of anodic peak current and ΔEp derived from CVs recorded with pyrolytic carbon microelectrodes fabricated with different pyrolysis heating rates and dwell times in 10 mM $[Fe(CN)_6]_{4-}$/$[Fe(CN)_6]_{3-}$ in PBS, scan rate 100 mV/s.

Pyrolysis conditions	Anodic peak current (μA)	Cathodic peak current (μA)	ΔEp (mV)
900 °C, 2 h, 10 °C/min	288.3 ± 15.2	-253.4 ± 3.3	239.3 ± 9.8
1 h, 10 °C/min	348.3 ± 14.3	-364.4 ± 15.4	170.9 ± 10.6
3 h, 10 °C/min	359.5 ± 0.3	-375.7 ± 0.4	159.5 ± 2.8
5 h, 10 °C/min	374.9 ± 14.9	-390.1 ± 16.4	161.7 ± 11.7
1 h, 30 °C/min	350.5 ± 3.1	-364.8 ± 4.4	180.7 ± 7.3
3 h, 30 °C/min	352.1 ± 10.1	-366.2 ± 10.9	181.5 ± 4.4
5 h, 30 °C/min	352.5 ± 1.5	–368 ± 0.6	167.8 ± 5.4
1 h, 50 °C/min	345.2 ± 2.2	-354.7 ± 1.2	173.3 ± 6.5
3 h, 50 °C/min	363.5 ± 14.2	-378.3 ± 16.4	157.9 ± 10.2
5 h, 50 °C/min	378.5 ± 16.1	-392.3 ± 13.6	153 ± 11

confirmed that neither the dwell time nor the heating rate represented statistically significant parameters for peak current values, with all p-values being higher than 0.05 (Supplementary Material, S1). Compared to other work, the results indicate no significant change of surface area with increased heating rates. Recently Sharma et al. [26] showed that fast ramping rates (higher than 25 °C/min) lead to porous pyrolytic carbon surfaces. However, investigation of the electrode surfaces using SEM and AFM confirmed smooth pyrolytic carbon surfaces in our case.

Singh et al. performed cyclic voltammetry on pyrolytic carbon electrodes fabricated at 1100 °C using the same redox couple, but with different scan rates [14]. Comparing the peak current values from this study with our results, and taking into account the different working electrode areas and scan rates, we can conclude that the results are comparable.

For ΔE_p both time and heating rate had a small influence, where processes with longer dwell times and higher heating rates showed smaller ΔE_p values. This is confirmed by the p-values for the dwell time and heating rate squared, which are 0.05 and 0.04 respectively.

Combining the results obtained from the resistivity and the voltammetry measurements, the process that showed the best electrical and electrochemical properties was the 5 h process with a ramp of 50 °C/min. For this reason, the electrodes obtained with these parameters were used for further electrochemical characterization. Different scan rates and concentrations were used to assess the reversibility of the electron transfer. For reversible systems such as $[Fe(CN)_6]^{4-}$/[Fe

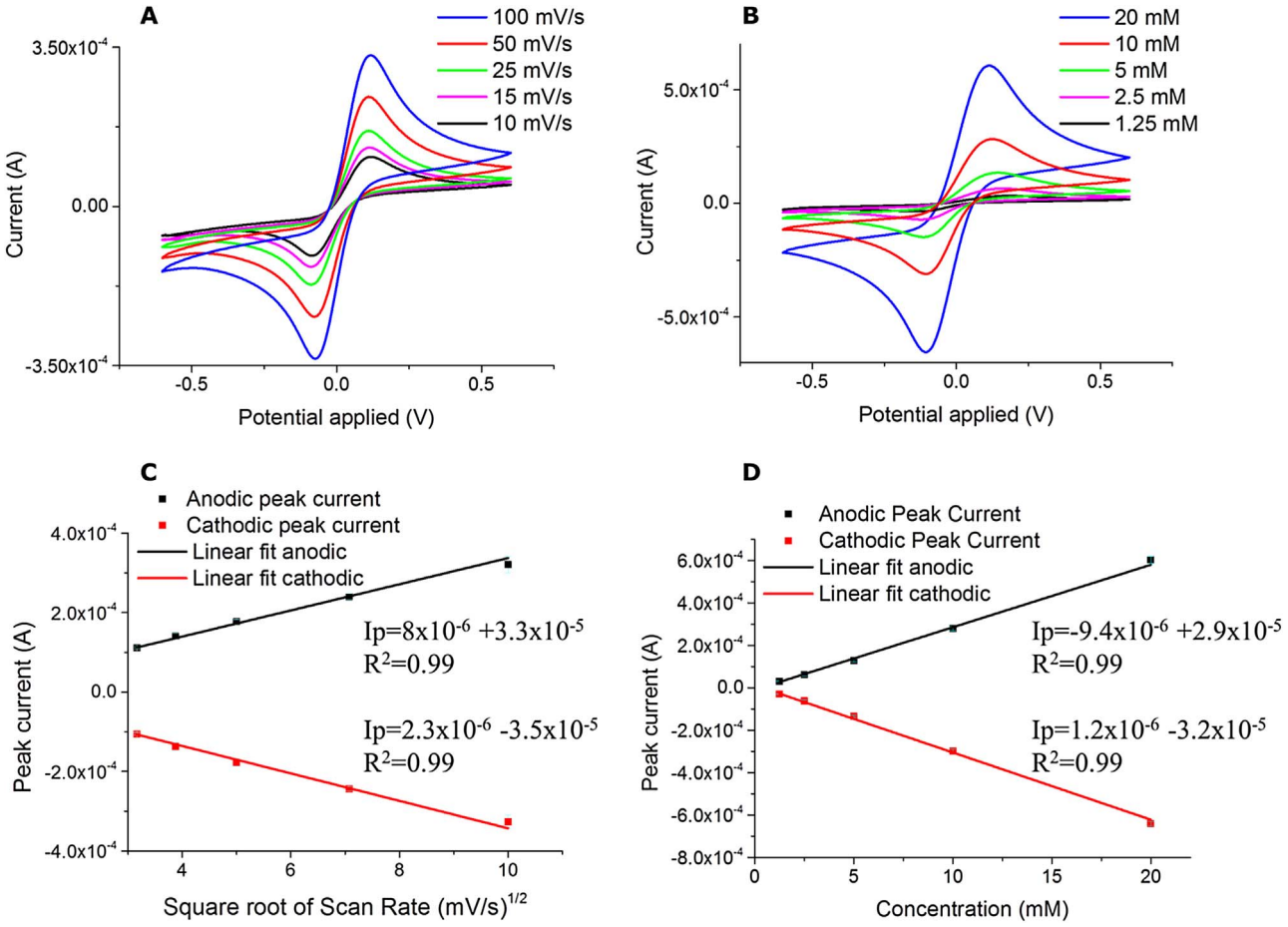

Fig. 8. Voltammograms of pyrolytic carbon electrodes obtained at 1100 °C (h = 50 °C/min, t = 5 h) acquired in 10 mM ferri-ferrocyanide varying scan rate (A) and concentration (B). Linear correlation between cathodic/anodic peak current and square root of scan rate (C) and the concentration (D).

$(CN)_6]^{3-}$ the peak currents should be directly proportional to the square root of the scan rate and concentration of the reactant, as described by the Randles-Sevcik equation [36].

Fig. 8 shows the cyclic voltammograms recorded with different scan rates (100 mV/s, 50 mV/s, 25 mV/s, 15 mV/s, 10 mV/s) (Fig. 8A) and concentrations of the redox probe $[Fe(CN)_6]^{4-}/[Fe(CN)_6]^{3-}$ (20 mM, 10 mM, 5 mM, 2.5 mM, 1.25 mM) (Fig. 8B) for the pyrolytic carbon electrodes. As shown in Fig. 8C and D, there was a linear relation of the peak current values with the square root of the scan rate and the redox probe concentration. Moreover, the ΔE_p remained constant, as expected for a reversible electron transfer reaction. This showed that the electrode reaction was diffusion controlled and that pyrolytic carbon films exhibit a similar electrochemical behavior as glassy carbon [37].

3.5. Electrochemical impedance spectroscopy

EIS has been used as additional method to characterize the electrochemical properties of the pyrolytic carbon electrodes. This technique allows the evaluation of the resistance of the electrochemical setup, which is dependent on the properties of the electrode material but also depends on the overall measurement setup. Furthermore, through the evaluation of the charge transfer resistance, it is possible to gather information about the electrochemical reaction rate. In Fig. 9 the Nyquist plots for electrodes obtained at 1100 °C are reported grouped by heating rates (10 °C/min, 30 °C/min, 50 °C/min). The graphs plot the imaginary impedance component (Z_{imag}) against the real impedance component (Z_{real}) at each excitation frequency. All the electrodes showed a similar behavior, with a small capacitive semicircle in the high frequency region, a larger semicircle and a straight line in the lower frequency region. The larger semicircle is a result of the electron-transfer kinetics of the redox probe at the electrode interface, while the linear part at lower frequency is due to diffusion-limited electron-transfer processes. The diameter of the larger semicircle gives an indication of the charge transfer resistance (R_{ct}), while the intercept with the real axis provides information on the solution resistance (R_{sol}) and the electrode conductivity [36]. For the samples pyrolyzed with a heating rate of 10 °C/min (Fig. 9A) longer dwell times led to a smaller charge transfer resistance. The same trend was observed for the heating rate of 50 °C/min where the 5 h process had the lowest R_{ct}. On the other hand, samples pyrolyzed with a heating rate of 30 °C/min showed no significant differences. An equivalent circuit, derived from a modified Randles model [38], was used to fit the impedance spectra obtained with different pyrolysis processes. Fig. 10 shows the equivalent circuit used (inset) and the fitting for a representative Nyquist plot of an electrode obtained with a pyrolysis process of 5 h at 1100 °C with a heating rate of 50 °C/min. R_b and C_b are the resistance and capacitance which are used to model the capacitive semi-circle in the high frequency region. R_{sol} represents the solution resistance, Y the magnitude of the constant phase element (CPE), *n* the multiplication factor of the phase angle, R_{ct} the charge transfer resistance and W the Warburg impedance. Fig. 10 shows that throughout the entire frequency range the circuit provides an excellent fit to the experimental data.

The values extracted from the fitting are reported in Table 3. R_b and C_b are related to the bulk properties of pyrolytic carbon but also contain contributions of the overall electrochemical setup (e.g. contact resistances, parasitic capacitances) [38]. Sp^2 and sp^3 regions inside the pyrolytic carbon lead to distributed resistances and capacitances. Higher values of R_b and C_b could be explained with larger sp^3 areas

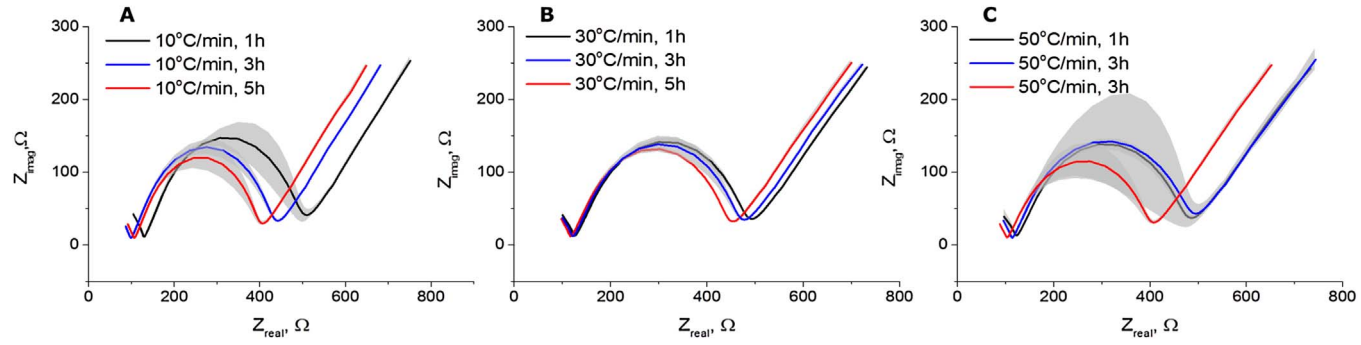

Fig. 9. Impedance spectra of pyrolytic carbon electrodes obtained with different dwell times at 1100 °C and different heating rates: 10 °C/min(A), 30 °C/min (B) and 50 °C/min (C) acquired in 10 mM ferri-ferrocyanide. Data are presented as mean ± standard deviation (n = 3).

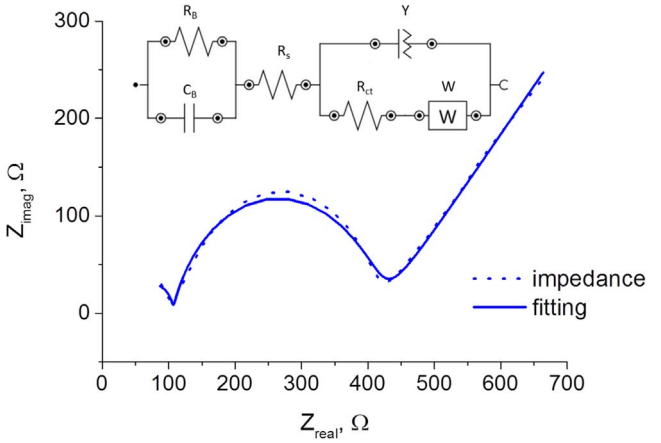

Fig. 10. Nyquist plot of carbon electrode obtained at 5 h at 1100 °C in N_2 with a heating rate of 50 °C/min. Inset shows the corresponding equivalent circuit model.

(insulating) resulting in a less conductive material. Table 3 shows that the values are in excellent agreement with the resistivity measurement performed with the Van der Pauw method, demonstrating a decrease of the R_b values when the dwell time is increased. However this trend is not observable for C_b and the main reason could be related with the equivalent circuit used: the part of the circuit composed of R_b and C_b might also be influenced by the resistance and capacitance contribution of the electrochemical setup. This kind of contribution should in principle be constant, but small variation can occur (e.g. leads and cable resistances). For this reason, in the opinion of the authors, trying to attribute an exact correlation between R_b, C_b and the pyrolytic carbon material properties might be error-prone. R_{sol} values represent the solution resistance, which in principle should be independent of the electrode material and as expected show small differences for the different pyrolysis processes. The 5 h process with the 50 °C/min heating rate showed the lowest R_{ct} value, meaning that it provided a better electron transfer compared to the other electrodes. Among others, this parameter is related to the surface area of the electrode and a rougher surface leads to lower R_{ct} values [39]. However, the differences between the various processes were small, meaning that electron transfer reaction rates were very similar, as confirmed by the comparable *n* values. The multiplication factor of the phase angle provides an indication of the roughness of the electrode surface, where a decreasing value of this parameter would indicate a more porous surface, and thus different electron transfer mechanisms [38]. AFM images were acquired to investigate the surface morphology of pyrolytic carbon obtained with different pyrolysis processes (Supplementary material S3). The root-mean square roughness measured by AFM was 1.6 nm for the samples pyrolyzed for 5 h at 50 °C/min, 1.4 nm for 30 °C/min and 1 nm for 10 °C/min. These values are similar to the ones obtained in earlier studies on pyrolysed photoresists [1,13,20] .Slower heating rates might provide more time to the photoresist to release the internal gases (O and H in SU-8 structure) in order to obtain a surface with a negligible roughness [12]. On the other hand, higher heating rates would not allow this controlled gas release, and consequently lead to a rough surface due to formation of small bubbles containing the unreleased gases [26]. In our case the fastest heating ramp of 50 °C/min led to a surface which is was only slightly rougher compared to the one obtained with the slowest heating rate of 10 °C/min. Nevertheless, these results are in accordance with the electrochemical ones, where the comparable R_{ct} and *n* values could be explained by the small surface roughness variations between samples obtained with different heating rates.

4. Conclusions

In this work, we focused on the improvement and characterization of 2D carbon electrodes obtained from negative epoxy based photoresist SU-8 with a pyrolysis process at 1100 °C in N_2. The influence of pyrolysis parameters such as heating rate and dwell time at the maximum temperature was investigated.

Table 3
Values (average ± standard deviation, n = 3) obtained from the fitting of the acquired impedance spectra. C_B and R_B are the capacitance and resistance, respectively, corresponding to the incomplete capacitive semi-circle at high frequencies; R_{sol} is the solution resistance; Y is the magnitude of the constant phase element (CPE) and n is a constant between 1 and 0; R_{ct} t is the charge transfer resistance; W is the Warburg impedance.

	C_B (nF)	R_B (Ω)	R_{sol} (Ω)	Y (μMho)	*n*	R_{ct} (Ω)	W (mMho)
1 h,10 °C/min	1.35 ± 0.02	84.3 ± 2.1	46.2 ± 1.1	4.8 ± 1.5	0.82 ± 0.023	369.1 ± 63	3.6 ± 0.04
3 h,10 °C/min	2.09 ± 0.25	51.4 ± 4.4	48.6 ± 2.3	3.8 ± 0.2	0.82 ± 0.006	333.8 ± 22.2	3.7 ± 0.02
5 h,10 °C/min	2.1 ± 0.06	55.4 ± 4	52.8 ± 0.9	3.1 ± 0.1	0.84 ± 0.002	339.6 ± 49.5	3.6 ± 0.05
1 h,30 °C/min	1.47 ± 0.09	80.2 ± 6.4	46.3 ± 1.1	4.1 ± 0.1	0.81 ± 0.004	358.1 ± 13.3	3.7 ± 0.02
3 h,30 °C/min	1.57 ± 0.09	73.3.3	49.4 ± 1.7	3.9 ± 0.2	0.82 ± 0.006	369 ± 46.5	3.6 ± 0.06
5 h,30 °C/min	1.51 ± 0.06	71.6 ± 1.9	46.5 ± 0.6	3.5 ± 0.2	0.82 ± 0.005	327.7 ± 7.9	3.6 ± 0.06
1 h,50 °C/min	1.85 ± 0.66	74.6 ± 24.4	48.5 ± 2	4.5 ± 0.1	0.80 ± 0.004	355.4 ± 19.5	3.6 ± 0.05
3 h,50 °C/min	1.64 ± 0.11	67 ± 1.8	47.6 ± 2.8	5.2 ± 1.1	0.82 ± 0.018	370 ± 142.6	3.5 ± 0.14
5 h,50 °C/min	1.80 ± 0.14	58.1 ± 0.7	45.5 ± 2.7	4.4 ± 1.3	0.80 ± 0.03	296.7.2 ± 46.6	3.6 ± 0.05

The obtained pyrolytic carbon showed excellent electrical properties, with lowest resistivity value of 3.2 ± 0.3 mΩcm. The resistivity values reported here are to our best knowledge the lowest ones reported for pyrolyzed photoresist films [11,12]. Furthermore, the carbon electrodes exhibit a glassy carbon-like electrochemical behavior, with a diffusion controlled electrode process. The fabrication process showed high reproducibility, confirmed by the low standard deviation values and the similar values of the two center points of the experimental design.

The influence of the different parameters was smaller than expected if compared to what has been shown in previous studies, where the variation of pyrolysis parameters such as heating rate led to significant changes in the surface porosity of pyrolytic carbon [26].

Nevertheless, it was possible to identify a trend in the resistivity measurements, showing that for processes carried out with heating rates of 10 °C/min and 50 °C/min longer dwell times led to lower resistivity values. The same trend was observable with cyclic voltammetry and impedance spectroscopy, where the best results were obtained for the process carried for 5 h and 50 °C/min. The statistical fitting of the results confirmed that the dwell time is the most influencing parameter for the electrical and electrochemical properties. On the other hand, for the thickness after pyrolysis the heating rate is the most relevant parameter. In this case, the already considerable shrinkage during pyrolysis is increased for higher heating rates, with the lowest carbon thickness values reported for the 50 °C/min processes.

This systematic study of different process parameters improves our understanding of the correlation between pyrolysis conditions and pyrolytic carbon material properties. Therefore, the results reported here can be useful for other future studies regarding the pyrolysis of polymer precursors to finely tune the pyrolytic carbon properties.

Acknowledgments

The authors acknowledge funding by the Young Investigator Program of the Villum Foundation, project no. VKR023438.

Mikkel Dysseholm Mar and Pernille Voss Larsen from DTU Danchip are acknowledged for the help with the pyrolysis process. Jesper Scheel is acknowledged for taking the pictures of the electrodes. Simon Pitscheider is acknowledged for the help with the AFM analysis.

Appendix A. Supplementary data

Supplementary data associated with this article can be found, in the online version, at http://dx.doi.org/10.1016/j.jaap.2017.04.015.

References

[1] R.L. McCreery, Advanced carbon electrode materials for molecular electrochemistry, Chem. Rev. 108 (2008) 2646–2687, http://dx.doi.org/10.1021/cr068076m.
[2] D.A.C. Brownson, C.W. Foster, C.E. Banks, The electrochemical performance of graphene modified electrodes: an analytical perspective, Analyst 137 (2012) 1815–1823, http://dx.doi.org/10.1039/c2an16279b.
[3] Y. Zheng, Y. Jiao, Y. Zhu, L.H. Li, Y. Han, Y. Chen, A. Du, M. Jaroniec, S.Z. Qiao, Hydrogen evolution by a metal-free electrocatalyst, Nat. Commun. 5 (2014) 1–8, http://dx.doi.org/10.1038/ncomms4783.
[4] J. Liang, Y. Zheng, J. Chen, J. Liu, D. Hulicova-Jurcakova, M. Jaroniec, S.Z. Qiao, Facile oxygen reduction on a three-dimensionally ordered macroporous graphitic C 3N 4/carbon composite electrocatalyst, Angew. Chem. Int. Ed. 51 (2012) 3892–3896, http://dx.doi.org/10.1002/anie.201107981.
[5] F. Bonaccorso, L. Colombo, G. Yu, M. Stoller, V. Tozzini, R.S. Ferrari, V. Pellegrini, 2D materials. Graphene, related two-dimensional crystals, and hybrid systems for energy conversion and storage, Science 347 (2015) 1246501, http://dx.doi.org/10.1126/science.1246501.
[6] L.L. Zhang, R. Zhou, X.S. Zhao, Carbon-based materials as supercapacitor electrodes, J. Mater. Chem. 38 (2009) 2520–2531, http://dx.doi.org/10.1039/c000417k.
[7] A.L. Beilby, A. Carlsson, A pyrolytic carbon film electrode for voltammetry, J. Electroanal. Chem. Interfacial Electrochem. 248 (1988) 283–304, http://dx.doi.org/10.1016/0022-0728(88)85091-5.
[8] Y. Matsuo, K. Iwasa, Y. Sugie, A. Mineshige, H. Usami, Preparation of carbon-based transparent and conductive thin films by pyrolysis of silylated graphite oxides, Carbon N. Y. 48 (2010) 4009–4014, http://dx.doi.org/10.1016/j.carbon.2010.07.004.
[9] K. Torbensen, J. Iruthayaraj, M. Ceccato, M. Kongsfelt, T. Breitenbach, S.U. Pedersen, K. Daasbjerg, Conducting and ordered carbon films obtained by pyrolysis of covalently attached polyphenylene and polyanthracene layers on silicon substrates, J. Mater. Chem. 22 (2012) 18172, http://dx.doi.org/10.1039/c2jm32935b.
[10] J. Kim, X. Song, K. Kinoshita, M. Madou, B. White, Electrochemical studies of carbon films from pyrolyzed photoresist, J. Electrochem. Soc. 145 (1998) 2314–2319, http://dx.doi.org/10.1149/1.1838636.
[11] S. Ranganathan, R. McCreery, S.M. Majji, M. Madou, Photoresist-derived carbon for microelectromechanical systems and electrochemical applications, J. Electrochem. Soc. 147 (2000) 277, http://dx.doi.org/10.1149/1.1393188.
[12] B.Y. Park, L. Taherabadi, C. Wang, J. Zoval, M.J. Madou, Electrical properties and shrinkage of carbonized photoresist films and the implications for carbon microelectromechanical systems devices in conductive media, J. Electrochem. Soc. 152 (2005) J136, http://dx.doi.org/10.1149/1.2116707.
[13] S. Ranganathan, R.L. McCreery, Electroanalytical performance of carbon films with near-atomic flatness, Anal. Chem. 73 (2001) 893–900, http://dx.doi.org/10.1021/ac0007534.
[14] A. Singh, J. Jayaram, M. Madou, S. Akbar, Pyrolysis of negative photoresists to fabricate carbon structures for microelectromechanical systems and electrochemical applications, J. Electrochem. Soc. 149 (2002) 78–83, http://dx.doi.org/10.1149/1.1436085.
[15] W. Zhang, S. Zhu, R. Luque, S. Han, L. Hu, G. Xu, Recent development of carbon electrode materials and their bioanalytical and environmental applications, Chem. Soc. Rev. 45 (2016) 715–752, http://dx.doi.org/10.1039/C5CS00297D.
[16] C. Wang, L. Taherabadi, G. Jia, M. Madou, Y. Yeh, B. Dunn, C-MEMS for the manufacture of 3D microbatteries, Electrochem. Solid-State Lett. 7 (2004) A435, http://dx.doi.org/10.1149/1.1798151.
[17] G.T. Teixidor, C. Wang, M. Madou, Fabrication of 3D carbon microelectrodes for Li-Ion battery applications, Nanoscale Fabr. 3 (2006) 221–224.
[18] G.T. Teixidor, R. a Gorkin, P.P. Tripathi, G.S. Bisht, M. Kulkarni, T.K. Maiti, T.K. Battacharyya, J.R. Subramaniam, A. Sharma, B.Y. Park, M. Madou, Carbon microelectromechanical systems as a substratum for cell growth, Biomed. Mater. 3 (2008) 34116, http://dx.doi.org/10.1088/1748-6041/3/3/034116.
[19] H. Xu, K. Malladi, C. Wang, L. Kulinsky, M. Song, M. Madou, Carbon post-microarrays for glucose sensors, Biosens. Bioelectron. 23 (2008) 1637–1644, http://dx.doi.org/10.1016/j.bios.2008.01.031.
[20] J.A. Lee, S. Hwang, J. Kwak, S. Il Park, S.S. Lee, K.C. Lee, An electrochemical impedance biosensor with aptamer-modified pyrolyzed carbon electrode for label-free protein detection, Sens. Actuators B Chem. 129 (2008) 372–379, http://dx.doi.org/10.1016/j.snb.2007.08.034.
[21] J.A. Lee, S.S. Lee, K.C. Lee, S. Il Park, B.C. Woo, J.O. Lee, Biosensor utilizing resist-derived carbon nanostructures, Appl. Phys. Lett. 90 (2007), http://dx.doi.org/10.1063/1.2752719.
[22] L. Amato, A. Heiskanen, C. Caviglia, F. Shah, K. Zór, M. Skolimowski, M. Madou, L. Gammelgaard, R. Hansen, E.G. Seiz, M. Ramos, T.R. Moreno, A. Martínez-Serrano, S.S. Keller, J. Emnéus, Pyrolysed 3D-carbon scaffolds induce spontaneous differentiation of human neural stem cells and facilitate real-time dopamine detection, Adv. Funct. Mater. 24 (2014) 7042–7052, http://dx.doi.org/10.1002/adfm.201400812.
[23] R. Martinez-Duarte, P. Renaud, M.J. Madou, A novel approach to dielectrophoresis using carbon electrodes, Electrophoresis 32 (2011) 2385–2392, http://dx.doi.org/10.1002/elps.201100059.
[24] O.J.A. Schueller, S.T. Brittain, G.M. Whitesides, Fabrication of glassy carbon microstructures by pyrolysis of microfabricated polymeric precursors, Adv. Mater. 9 (1997) 477-, http://dx.doi.org/10.1002/adma.19970090604.
[25] A. Mardegan, R. Kamath, S. Sharma, P. Scopece, P. Ugo, M. Madou, Optimization of carbon electrodes derived from epoxy-based photoresist, J. Electrochem. Soc. 160 (2013) B132–B137, http://dx.doi.org/10.1149/2.107308jes.
[26] S. Sharma, R. Kamath, M. Madou, Porous glassy carbon formed by rapid pyrolysis of phenol-formaldehyde resins and its performance as electrode material for electrochemical double layer capacitors, J. Anal. Appl. Pyrolysis. 108 (2014) 12–18, http://dx.doi.org/10.1016/j.jaap.2014.05.025.
[27] L.J. van der Pauw, A method of measuring the resistivity and Hall coefficient on lamellae of arbitrary shape, Philips Tech. Rev. 20 (1958) 220–224. 537.723.1:53.081.7 + 538.632:083.9.
[28] D.M.A. Mackenzie, J.D. Buron, P.R. Whelan, B.S. Jessen, A. Silajdźić, A. Pesquera, A. Centeno, A. Zurutuza, P. Bøggild, D.H. Petersen, Fabrication of CVD graphene-based devices via laser ablation for wafer-scale characterization, 2, D Mater . 2 (2015) 45003, http://dx.doi.org/10.1088/2053-1583/2/4/045003.
[29] D.C. Montgomery, Design and Analysis of Experiments, Eight edit, John Wiley & Sons Inc., 2013.
[30] Y. Mohamed Hassan, C. Caviglia, S. Hemanth, D.M.A. Mackenzie, D.H. Petersen, S.S. Keller, Pyrolytic carbon microelectrodes for impedance based cell sensing, ECS Trans. 72 (2016) 35–44.
[31] S. Hemanth, C. Caviglia, L. Amato, T.A. Anhøj, A. Heiskanen, J. Emnéus, S.S. Keller, Pyrolytic 3D carbon microelectrodes for electrochemistry, ECS Trans. 72 (2016) 117–124.
[32] F. Tuinstra, L. Koenig, Raman spectrum of graphite, J. Chem. Phys. 53 (1970) 1126–1130, http://dx.doi.org/10.1063/1.1674108.
[33] A. Ferrari, J. Robertson, Interpretation of Raman spectra of disordered and amorphous carbon, Phys. Rev. B. 61 (2000) 14095–14107, http://dx.doi.org/10.1103/PhysRevB.61.14095.
[34] R. Kostecki, B. Schnyder, D. Alliata, X. Song, K. Kinoshita, R. Kötz, Surface studies of

carbon films from pyrolyzed photoresist, Thin Solid Films 396 (2001) 36–43, http://dx.doi.org/10.1016/S0040-6090(01)01185-3.
[35] P.J.F. Harris, Fullerene-related structure of commercial glassy carbons, Philos. Mag. 84 (2004) 3159–3167, http://dx.doi.org/10.1080/14786430410001720363.
[36] A.J. Bard, L.R. Faulkner, Electrochemical methods: fundamentals and applications, Wiley, 2001.
[37] I. Hu, D.H. Karweik, T. Kuwana, Activation and deactivation of glassy carbon electrodes, J. Electroanal. Chem. 188 (1985) 59–72, http://dx.doi.org/10.1016/S0022-0728(85)80050-4.
[38] L. Amato, A. Heiskanen, R. Hansen, L. Gammelgaard, T. Rindzevicius, M. Tenje, J. Emnéus, S.S. Keller, Dense high-aspect ratio 3D carbon pillars on interdigitated microelectrode arrays, Carbon N. Y. 94 (2015) 792–803, http://dx.doi.org/10.1016/j.carbon.2015.06.014.
[39] V.F. Lvovich, Impedance Spectroscopy, John Wiley & Sons, Inc., Hoboken, NJ, USA, 2012, http://dx.doi.org/10.1002/9781118164075.